Slanted septum and multiple folded cavity liners for broadband sound absorption

Journal Title
XX(X):2–29
©The Author(s) 2016
Reprints and permission:
sagepub.co.uk/journalsPermissions.nav
DOI: 10.1177/ToBeAssigned
www.sagepub.com/
SAGE

Suresh Palani[1], Paul Murray[1], Alan McAlpine[1], Daisuke Sasaki[2], and Christoph Richter[3]

Abstract

The design of acoustic liners with complex cavities for a wide frequency range of attenuation using numerical method is investigated in this paper. Three novel liner concepts are presented, demonstrating predicted improvements in broadband sound absorption when compared with that for conventional designs. The liners include a slanted septum core, a slanted septum core with varying percentage open area, and a MultiFOCAL concept. A finite element model of a normal incidence impedance tube is developed using COMSOL Multiphysics modeling software to predict the acoustic properties (resistance and reactance) of liners at medium and high sound pressure levels, and to study the impact of variations in the liner design parameters. The impedance tube finite element model incorporates non-linear semi-empirical impedance equations, validated by comparing numerical results with measurements performed on a single-degree-of-freedom liner, with a perforated face sheet, at high sound pressure level. The design variables of the novel liner concepts are optimized using a hybrid automated optimisation procedure. The low-frequency optimum slanted septum core concept with an open area of 4.5 % for the face sheet and 18 % for the short slanted septum is predicted to have an absorption level of at least 14 dB in the frequency range of 400–1000 Hz for normally incident pure tone excitations at 150 dB. The slanted septum core concept with varying percentage open area, with broadband optimum design variables, is predicted to have good broadband sound absorption levels of at least 10 dB in the frequency range of 570–3800 Hz. Finally, the MultiFOCAL liner concept with optimised percentage open areas is predicted to have an excellent broadband sound absorption levels of at least 14 dB, for pure tone excitations at 150 dB, in the frequency range of 900–5300 Hz. This work will be followed by optimisation of the face sheet geometries of these novel liner designs in order to maximise lined duct attenuation for aircraft engine applications.

Keywords

Novel liners, multiple folded cavities, perforated slanted septum, high SPL, optimization, broadband sound absorption

Introduction

Noise and CO_2 emissions are key characteristics of aero-engines, as they enable public acceptance of growing air traffic. For decades reductions of noise and CO_2 emissions were achieved by increasing the bypass ratio, based on Lighthill's pioneering work in 1952. Today, further reductions require optimisation of all components which contribute to the noise signature. This work will focus the optimisation potential of the acoustic treatment. In future aero-engines, even with the most advanced technologies for noise reduction at the source, there will be a continuing demand for passive noise reduction by acoustic liners. More effective designs of acoustic liners are required for passive noise control to achieve the envisaged noise and CO_2 emissions targets of the ACARE Flightpath 2050.

Theoretical and experimental studies have provided significant knowledge on the working principle of single-degree-of-freedom (SDOF) liners[1–6]. Engine duct and liner parameters such as mean flow/boundary layer thickness, liner resistive sheet geometry and cell depth, and incident sound pressure level, have all been recognized to affect the noise attenuation of acoustic liners. Empirical and semi-empirical models predicting the installed impedance of acoustic liners are documented in the scientific literature[3,6–8]. However, there have been relatively few attempts to investigate the dedicated design of liner resistive sheets and cavity geometries for sound absorption over a broad range of frequencies. Jones and Parrott[9] developed a group of parallel-element, narrow-chamber liners constructed from ceramic tubular material with an effective percentage of open area (POA_{eff}) of 57 %. The impedance of this novel concept liner was evaluated using the NASA normal incidence test set-up. Impedance prediction models were also developed based on the transmission line model[9]. These narrow-chamber liners derive their acoustic resistance from viscous losses within the narrow chambers. Jones et al.[10] developed a new liner treatment concept called a multi-layer liner, with mesh-caps. This concept allows the acoustic liner to be customized such that the impedance of each individual cell is independently controlled. This is achieved by selecting the combination of liner parameters to set the impedance in each cell. Schiller and Jones[11] subsequently developed a broadband liner design concept called a variable depth liner, composed of groups of resonators tuned for different frequencies.

Only recently has greater attention been devoted to the design of complex cavities to attain optimum acoustic impedance for aero-engine noise reduction at lower frequencies. Rie et al.[12] investigated the design and performance of folded cavity liners for turbofan engine inlets. The design of complex cavities appears to be an inevitable step in the evolution of acoustic liners for larger aero-engines, due to the large spread of source frequencies to be attenuated and the impact of cross section on drag and weight of the liner. Also today, additive manufacturing processes make complex acoustic liner designs feasible[7,13–15].

[1] Institute of Sound and Vibration Research, University of Southampton, Southampton, UK.
[2] Department of Aeronautics, Kanazawa Institute of Technology, Ishikawa, Japan.
[3] Rolls-Royce Deutschland Ltd & Co KG, Dahlewitz, Eschenweg 11, 15827 Blankenfelde-Mahlow, Germany.

Corresponding author:
Suresh Palani, Institute of Sound and Vibration Research, University of Southampton, Southampton, SO17 1BJ, UK.
Email: S.Palani@soton.ac.uk

Prepared using sagej.cls

The aim of this initial work is to develop novel acoustic liner concepts with improved normal incidence broadband absorption using a finite element (FE) impedance tube test model developed using the COMSOL Multiphysics modeling software. Particular interest will be on the design of the liner cavity with complex internal structures. The main advantage of the FE method lies in its ability to accurately simulate the physical processes involved in the sound absorption mechanism of acoustic liners, and offer detailed insights that can complement the knowledge gained from theoretical and experimental approaches. Also, the frequency domain approach is also much less expensive compared to the time domain approach in terms of the computational time, although only a single frequency can be computed at a time.

The computational model

A two-dimensional impedance tube of length L is modelled using COMSOL Multiphysics to predict the normal incidence impedance of acoustic liners of cavity height H_c in the absence of grazing flow. **Figure 1** shows a schematic of a 2-D impedance tube finite element model used in this study. A plane wave radiation boundary is defined at the top of the impedance tube, at $y = L + H_c$. The amplitude of the incident pure tone plane waves is iterated until the target value is reached at the face sheet of the liner, at $y = H_c$. The impedance tube and the cavity is then meshed with quadratic elements.

Considering the requirement for purely plane wave propagation inside the modelled 2-D impedance tube, the maximum frequency range of interest for a 29 mm diameter (D) tube is ≈ 6930 Hz. In order to minimize the influence of evanescent modes, this upper limit is reduced to 6400 Hz. The lower frequency limit is zero for traditional sample holder impedance tube measurements. When the model is used to represent flanged impedance tube measurements, a lower limit is identified which is driven by the mismatch in area between the tube and the 'visible' cavity (driven by the liner honeycomb cell width).

In this article the COMSOL FE model is used to design novel acoustic liners with complex geometries, which are optimized for maximum sound absorption at normal incidence. The frequency domain model employs semi-empirical impedance equations for resistive layers, as the primary aim is to establish the effect of complex designs on the impedance. It should also be noted that the acoustic properties of the liners modelled here for the normal impedance test set-up is a simple case without grazing flow. In practice, the impedance will be altered by the presence of a background grazing flow and a complex source consisting of a combination of tonal and broadband frequencies, typical of aero-engine operating conditions.

An assessment of the semi-empirical impedance equations used in the COMSOL FE model is also included. This is carried out by comparing the predicted normalised non-linear impedance with measurements of SDOF liner treatments with different perforated face sheets that are typical of those used in aircraft engine ducts. The specific resistance and reactance at the liner surface are computed by solving the Helmholtz equation for a given liner geometry and frequency. Although the governing equations are derived for small disturbances under the assumption of linear acoustics, the numerical model has the potential to simulate the non-linear acoustic properties of liners at high sound pressure levels. The non-linear acoustic properties of the liners are included in the governing interior boundary condition equations.

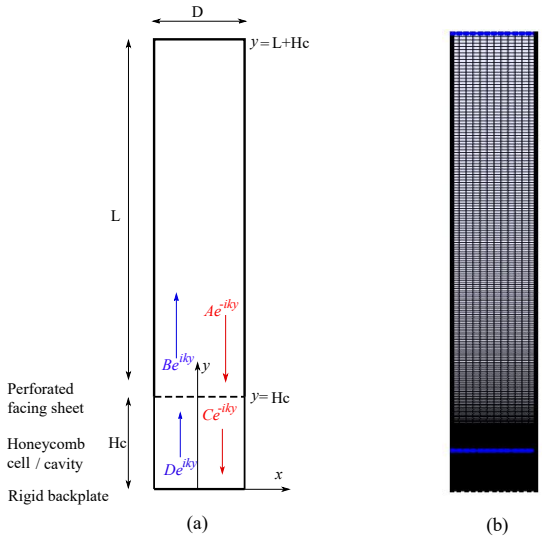

Figure 1. Schematic of impedance tube. a) Physical model and b) Finite Element model.

Governing Equations

In this study, the finite element modelling is based on linearisation of the equations governing the isentropic motion of an inviscid and adiabatic perfect gas. As a result, the mean speed of sound c_0 and density of air ρ_0 are constant. In the absence of background mean flow, i.e. $\mathbf{u}_0 = \mathbf{0}$, the resulting acoustic field equations, after ignoring the higher-order terms of small perturbations, are as follows:

Acoustic continuity

$$\frac{\partial \rho'}{\partial t} + \rho_0 \nabla . \mathbf{u}' = 0 \,, \tag{1}$$

Acoustic momentum

$$\rho_0 \frac{\partial \mathbf{u}'}{\partial t} + \nabla p' = 0 \,, \tag{2}$$

Acoustic energy

$$\frac{\partial p'}{\partial t} + \gamma p_0 \nabla . \mathbf{u}' = 0 \,. \tag{3}$$

where p', ρ', and $\mathbf{u}'$ are the acoustic pressure, density, and particle velocity fluctuations, respectively. In equation 3, γ is the ratio of specific heats at constant pressure (C_P) and volume (C_V).

Combining equations 1 to 3, the linearised acoustic wave equation describing the motion of acoustic pressure p' in the quiescent impedance tube model is given by,

$$\frac{\partial^2 p'}{\partial t^2} - c_0^2 \nabla^2 p' = 0 \,, c_0^2 = \gamma p_0 / \rho_0 \,. \tag{4}$$

For a time harmonic ($e^{i\omega t}$) acoustic perturbation, the linearised acoustic wave equation can be rewritten in the form of the linearised Helmholtz equation in the frequency domain as,

$$\nabla^2 p' + k^2 p' = 0\,, \tag{5}$$

where $k = \omega/c_0$ is acoustic free-field wave number.

The linearised Helmholtz equation 5 is converted to an equivalent integrated or weak statement formulation and then the weak formulation is discretised into finite elements using COMSOL[16].

Liner Impedance Model - Interior Boundary Condition

Semi-empirical impedance equations are implemented, for perforated face sheets, into the FE model in the form of interior impedance boundary conditions. The linear part of the acoustic resistance is due to the viscous scrubbing frictional losses inside the perforate holes. This is given by[3]

$$R_{\text{lin}} = \frac{\alpha \mu t_p}{2\rho_o c_o \left(\sigma C_D\right) {d_h}^2}\,, \tag{6}$$

where the resistance R is normalised by $\rho_0 c_0$. In equation 6, α is an empirical constant, μ is the dynamic viscosity of air, t_p is the face-sheet thickness, σ is the percentage open area (POA) ratio or porosity of the face sheet, C_D is the discharge coefficient, and d_h is the face sheet perforate hole diameter.

At medium and high sound pressure levels, the displacement of acoustic particles becomes comparable to the diameter of the holes, and vortices start shedding at the entrance and the exit of the perforation hole. This results in additional dissipation of acoustic energy, increasing the acoustic resistance of the perforate. Thus an additional non-linear resistance term is added to equation 6. The normalised non-linear acoustic resistance for the circular perforates is calculated as

$$R_{\text{non-lin}} = \frac{1-\sigma^2}{2c_0\sigma^2 C_D^2}|u_n|\,, \tag{7}$$

where $|u_n|$ is the surface acoustic particle velocity component normal to the perforated plate, $1-\sigma^2$ is an experimentally derived dimensionless entrance and exit loss coefficient of flow at the perforate orifice, and C_D is the hole discharge coefficient.

Apart from the non-linear resistance response, clear evidence of non-linearity in the face sheet reactance with respect to the sound pressure level (SPL) was observed by Hersh et al.[4], Murray and Astley[6] and Serrano et al.[7]. With increasing SPL, the face sheet reactance component reduces as the amplitude of the particle displacement through the perforate holes becomes greater than the hole diameter. The normalised non-linear perforate acoustic reactance is given by

$$X_{\text{non-lin}} = \frac{k(t_p + \epsilon\delta d_h)}{\sigma}\,, \tag{8}$$

where δ is the dimensionless non-linear correction for reactance deduced by using high amplitude impedance tube measurements[6], and ϵ is the dimensionless end correction proposed by Ingard[17]. For perforates, ϵ is given by

$$\epsilon = 0.85(1 - 0.7\sqrt{\sigma})\,. \tag{9}$$

Combining **Equations 7–8** gives the total normalised specific acoustic impedance of a thin perforated face sheet or septum

$$Z = \frac{\alpha \mu t_p}{2\rho_o c_o \left(\sigma C_D\right) {d_h}^2} + \frac{1-\sigma^2}{2c_0\sigma^2 C_D^2}|\hat{u}| + i\frac{k(t_p + \epsilon\delta d_h)}{\sigma} \,. \tag{10}$$

In the COMSOL FE model used for these studies, the boundary condition of the perforated face sheet is defined by **Equation 10**.

Impedance Calculation

For time-harmonic excitation, the total pressure field in the impedance tube can be expressed by

$$\tilde{P}(y) = \tilde{A}e^{jky} + \tilde{B}e^{-jky} \,, \tag{11}$$

where $\tilde{A}$ and $\tilde{B}$ are arbitrary complex constants which represent the amplitude and the relative phase of plane waves travelling in the positive and negative y direction, respectively. From the linearised equation of momentum conservation (Eqn. 2), the acoustic particle velocity is given by

$$\tilde{u}(y) = \frac{\tilde{A}e^{jky} - \tilde{B}e^{-jky}}{\rho_0 c_0} \,. \tag{12}$$

Therefore, the normalized specific acoustic impedance, from Eqn. 11 and Eqn. 12, is given by,

$$\tilde{Z}(y) = \frac{\tilde{P}(y)}{\tilde{u}(y)\rho_0 c_0} = \frac{\tilde{A}e^{jky} + \tilde{B}e^{-jky}}{\tilde{A}e^{jky} - \tilde{B}e^{-jky}} \,. \tag{13}$$

From Eqn. 13 the normalised acoustic impedance at the facing sheet is given by,

$$\tilde{Z}(H_c) = \frac{\tilde{A}e^{jkH_c} + \tilde{B}e^{-jkH_c}}{\tilde{A}e^{jkH_c} - \tilde{B}e^{-jkH_c}} \,. \tag{14}$$

The above expression for the impedance at the facing sheet is modified as the amplitudes of the incoming and outgoing waves cannot be measured at H_c. The total pressure at the inlet plane can be calculated from COMSOL. Assuming that the amplitude of the incoming time-harmonic plane wave has a known input value P_A and phase $\phi_A = 0$, the total pressure at the inlet ($y = L + H_c$) is given by

$$\tilde{P}(L + H_c) = \tilde{P}_i + \tilde{P}_r = P_A e^{jk(L+H_c)} + \tilde{B}e^{-jk(L+H_c)} \,. \tag{15}$$

The incoming and outgoing wave terms in Eqn. 14 can be re-written as,

$$\tilde{A}e^{jkH_c} = \tilde{A}e^{jk(L+H_c)}e^{-jkL} = P_A e^{jk(L+H_c)}e^{-jkL}, \tag{16}$$

and

$$\tilde{B}e^{-jkH_c} = \tilde{B}e^{-jk(L+H_c)}e^{jkL} = [\tilde{P}(L + H_c) - P_A e^{jk(L+H_c)}]e^{jkL}. \tag{17}$$

Substituting Eqn. 16 and 17 in Eqn. 14 gives the impedance at the liner face sheet,

$$\tilde{Z}(H_c) = \frac{P_A e^{jky} + [\tilde{P}(y) - P_A e^{jky}]e^{j2kL}}{P_A e^{jky} - [\tilde{P}(y) - P_A e^{jky}]e^{j2kL}} \,, \tag{18}$$

Equation 18 is implemented in the COMSOL FE model to calculate the impedance on the liner surface by defining the value of P_A and length of the impedance tube from the surface of the liner (L).

Validation for a SDOF Liner with Normal Incidence

The model developed in COMSOL is now validated using the experimental results for SDOF liners without grazing flow from Murray and Astley[6]. The perforate liners were identified as low POA (in the range of 3–6 %) and medium POA (in the range of 6–10 %). In each case, the predicted value of the incident sound pressure level at the face sheet is iterated until it matches with that of the measured values.

SDOF Liner with Low POA

The predicted pure tone response of the SDOF liner with low open area, for sound pressure levels of 130 dB, 140 dB and 150 dB, and for frequencies upto 6.4 kHz are compared with the measurements and shown in **Figure 2**.

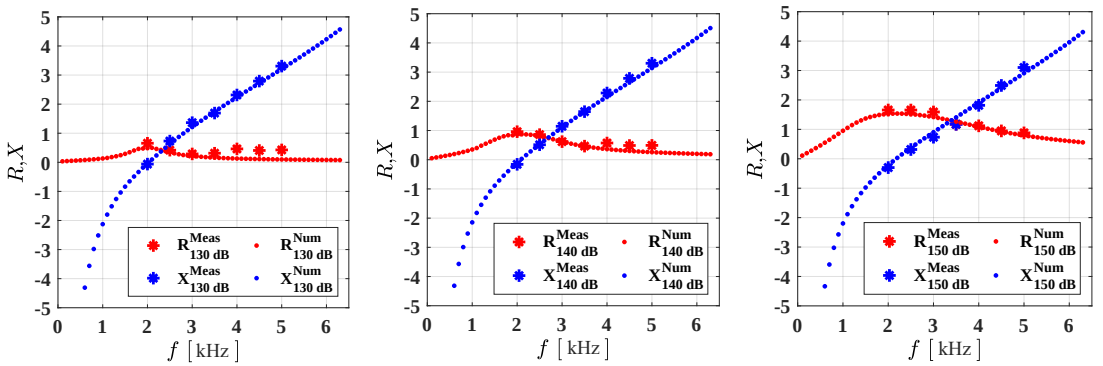

(a) 130 dB **(b)** 140 dB **(c)** 150 dB

Figure 2. Measured and predicted pure tone response of SDOF liner with low open area

It can be seen from **Figure 2** that both the measured and the predicted value of the resistance increases due to the increase in the incident sound pressure level. This verifies the results from the previous studies that at medium and high sound pressure levels acoustic dissipation is comprised of two components (as expressed in **Equation 10**): (1) the dominant shedding of small vortices for high hole acoustic velocities (non-linear part), and (2) the direct viscous dissipation near the liner opening (linear part).

SDOF Liner with Medium POA

In **Figure 3**, the predicted impedance of the SDOF liner with medium open area at 130 dB, 140 dB and 150 dB tonal sound amplitude, at frequencies upto 6.4 kHz, are compared with the pure tone response measured using a normal impedance tube. It is clear that the predicted resistance and reactance are in excellent agreement with the experimental results. The predicted value of the resistance increases due to the increase in the incident sound pressure level. It is also interesting to note that the non-linear resistance values of this medium POA SDOF liner are lower compared to those for the low POA SDOF liner. This is because the non-linear resistive part of a perforated face sheet is inversely related to the square of open area, as shown in **Equation 10**.

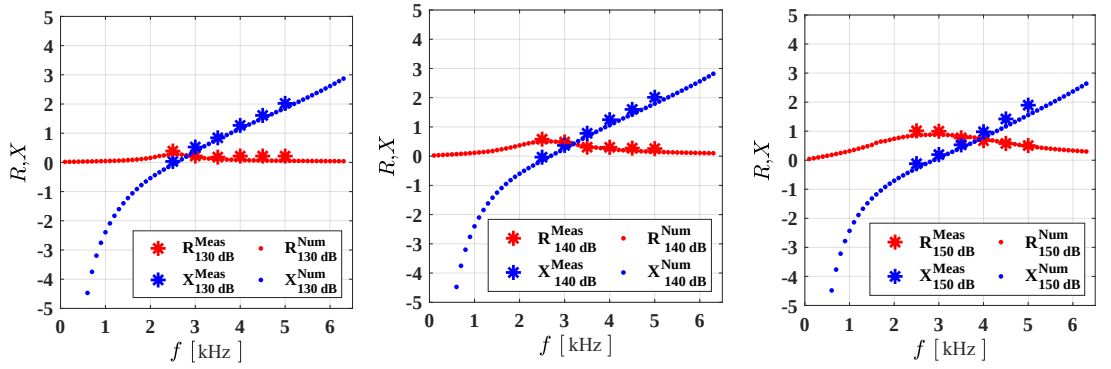

(a) 130 dB **(b)** 140 dB **(c)** 150 dB

Figure 3. Pure tone response of SDOF liner with medium open area

Automated Optimisation Procedure

Early work on the liner optimisation problem focused primarily on the reduction of fan noise radiation from commercial aircraft engine nacelles. Specifically, the liner impedance is used as a control variable in order to estimate the optimal value that minimizes far-field radiated noise. Lafronza et al.[18] developed an optimisation procedure, based on a response surface model, to investigate the design of both a uniform and an axially-segmented acoustic liner for a simplified aero-engine inlet model. In the first instance, design of experimental methods were used to build an ensemble sample of points used to develop a response surface model. Later, this surrogate model (RSM) was used for searching for optimum design solutions instead of the real model. A semi-analytic mode-matching method was used for characterising the acoustic propagation in the lined and the hard-walled part of the aero-engine duct model. An approximate Perceived Noise Level (PNL) calculation was used as an objective function.

Copiello et al.[19] developed an automated multi-objective procedure to optimize the design parameters of a zero-splice acoustic liner in a uniform cylindrical duct. The Non-Dominated Sorting Genetic Algorithm II[20] was applied to the optimisation problem to determine a set of candidate solutions for the final selection of the liner configuration. The component Effective Perceived Noise Levels (EPNL) at approach and flyover were calculated and used as cost functions. The cost functions were computed, assuming an engine fan model as a noise source, using analytical acoustic propagation and radiation models for each liner design.

Astley et al.[21] developed semi-automated and fully-automated computational aero-acoustic (CAA) procedures to optimize the barrel liner of an inlet at the approach condition. The finite element code ACTRAN/TM was used to predict the far-field sound pressure with and without the acoustic liner. The difference between the far-field sound pressure over a selected angular range, with and without the liner, was used as the cost function since propagation to selected directivity angles tends to dominate the EPNL at the approach condition. The fully automated optimisation procedure was based on a genetic algorithm (GA) multi-objective optimisation tool (ARMOGA) developed by Sasaki et al.[22].

Chambers et al.[23] developed an optimisation procedure to design innovative 3-D folded core geometries for acoustic liners, targeting low-frequency ($< 500\,\text{Hz}$) noise absorption. The relative performance of various 3-D folded core designs were compared using the low-frequency performance (LFP) metric. The liner impedance was predicted using the Zwikker–Kosten Transmission Line (ZKTL) model developed by Jones and Parrott[9]. The main objective of this optimisation was to find the best packing of 3-D folded cavities based on the LFP metric.

Tissot et al.[24] developed a numerical shape optimisation strategy based on an ad-joint method to design the cavity of a SDOF liner for very low frequency sound absorption. The shape of the cavity was modified in order to match a given target normal incidence impedance $Z = 1 + 0j$, corresponding to perfect absorption, for a given normalised frequency range.

In this current work, a COMSOL FE model is used, along with the semi-empirical equations, for the prediction of the impedance of resistive layers to predict the acoustic properties of novel liners subjected to a normal incidence plane wave. The predictions are performed using a 2-D impedance tube test set-up.

Cost Function

The objective of this optimisation problem is to determine the optimum percentage open area of the face sheet/sheets and septum/septa in order to minimize the average normal incidence sound pressure reflection coefficient ($\bar{\tau}$) for a given frequency range $\Delta f = f_j - f_i$. At each frequency within the range, the normal incidence complex reflection coefficient is calculated from

$$\tilde{\tau} = \frac{\tilde{Z} - 1}{\tilde{Z} + 1}\,, \tag{19}$$

where $\tilde{Z}$ is the normalised specific acoustic impedance of the liner calculated numerically from **Equation 18**. Furthermore, the normal incidence absorption levels are calculated from the reflection coefficient as follows

$$\Delta\text{SPL}_\tau = -20 \times log_{10}(\tilde{\tau})\,, \tag{20}$$

where positive values of ΔSPL_τ signify sound absorption, in dB.

The average normal incidence reflection coefficient for a frequency range $[f_i, f_j]$ is expressed using the cost function or fitness function, defined as follows

$$\bar{\tau} = \frac{1}{\Delta f} \int_{f_i}^{f_j} |\tilde{\tau}\,(f)\,|\,\mathrm{d}f \tag{21}$$

where the integral is evaluated using the trapezium rule in MATLAB[25]. Optimisations are performed at a specific range of target frequencies by using the GA solvers[25]. It is noted that no weighting is applied to the objective function.

Design Variables

One of the most important parameters that defines the impedance of a locally-reacting acoustic liner is the percentage open area (POA), σ, which consequently has a key influence on the layer resistance and reactance and subsequently on the attenuation properties of the liner. As shown in **Figure 4**, the perforate holes of circular cross-section are uniformly distributed over the face sheet, and the POA is the ratio of

the open area to the total area of the plate. For a regular square pitch pattern, the percentage open area is defined as

$$\sigma = \frac{\pi {d_h}^2}{4p^2}\ , \tag{22}$$

where p is the centre to centre distance between the holes. The geometrical parameters of the liners such as the thickness of the face sheet (t_p) or septum, hole diameter (d_h), and overall thickness of the liner (H_c), are kept constant in this study.

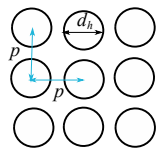

Figure 4. Schematic of perforated face sheet or septum.

Optimisation Scheme

An automated hybrid optimisation procedure is used to determine the optimum percentage open area (POA) of the face sheet/septa for novel liner concepts at high SPLs. The flow chart of the optimisation procedure is presented in **Figure 5**. Acoustic calculations are performed using the COMSOL FE model

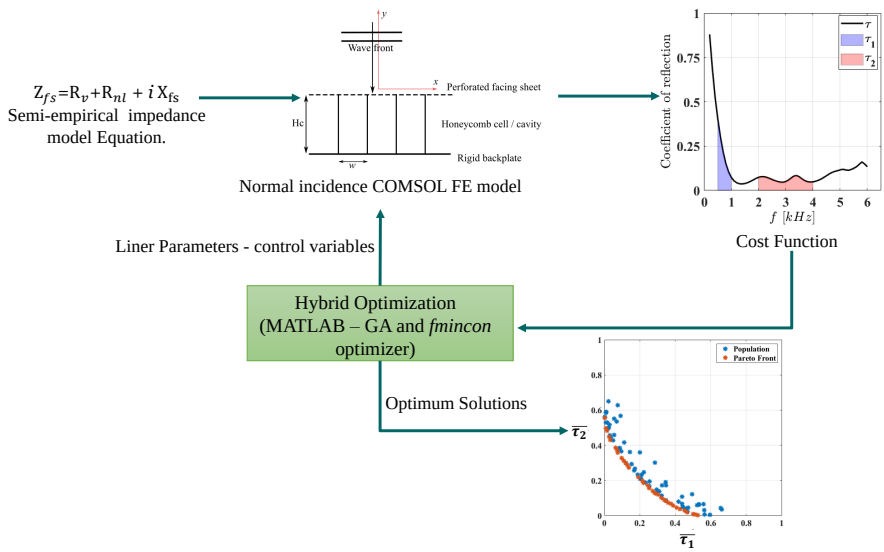

Figure 5. Flow chart for the novel liner design variable optimisation.

where a pure tone plane wave is normally incident upon the liner surface with a sound pressure level of 150 dB.

One of the most important inputs to the optimisation procedure is the liner configuration. Firstly, novel liners with complex cavities are designed using the COMSOL FE model to reduce noise over a relatively large bandwidth. The depth of the cavity (H_c) of the novel liners is maintained as low as possible (set nominally to 60 mm) to allow for potential installation inside an aero-engine nacelle. Secondly, optimum solutions are searched using the genetic algorithm (GA) and fmincon functions for single objective calculations, and gamultiobj function for multi-objective calculations, in MATLAB[25]. In future work, it is planned to build and test some of the optimum novel liner concepts that are presented in this article.

Single Objective Optimisation The average normal incidence sound pressure reflection coefficient, as given in **Equation 21**, for a specific novel liner concept is calculated for frequencies between 400 Hz and 6 kHz(step 100Hz), and set as the objective function. This singular objective function is then minimised by using a hybrid optimisation scheme which is a combination of an evolution based genetic algorithm (GA) and the gradient-based fmincon optimizer in MATLAB. In a similar approach, Astley et al.[21] has shown that the process of combining two optimisation solvers operated in sequence speeds the solution process.

The GA is an optimum solution search solver that evaluates the objective function for a set of random initial design variables, called the *initial population*, within the bounded limits. The initial population of the design variables in the current optimisation problem is uniformly distributed between the lower and upper limit. The lower limit of the design variable (POA) is set as $1\,\%$, approaching a hard-wall condition, and the upper limit is set as $20\,\%$, representing a highly-porous condition. Thus, the initial population of design variables includes a realistic range of porosities that may be used in acoustic liners for an aero-engine nacelle application.

The algorithm then creates a new set of populations, called "children", from a subset of individual design variables, called "parent", from the current *population* through mutation and cross-over processes[25]. In general, the algorithm tends to select parents that have the minimum cost function value, in the case of a minimization problem. This procedure is repeated iteratively until the populations of successive *generations* approach an optimum point/solution.

The accuracy of the optimum solution of a GA solver depends on the *population* size and the number of *generations*. The individual design variables in the population of the n^{th} generation approaches the optimum design solution as the value of n increases[25]. As a result, if only a GA is used for the optimisation, the evaluation of the cost function will become computationally expensive. In this study, a hybrid optimisation is applied to search for the best possible solution in the entire design space bounded by the limits, using a GA solver followed by using the *fmincon* solver[25]. A *population* size of 50, 75, and 100 design points is used with a number of *generations* ranging from 1 to 3 depending on the number of design variables required to be optimized. The number of design variables depends on the complexity of the novel liner concepts. The other settings of the GA solver options are retained with their default values.

The best solution of the last generation from the GA solver is passed on to *fmincon* as the initial point to perform a more efficient local search near the optimum point. The *fmincon* algorithm is a non-linear multi-objective gradient-based method which uses the "trust-region reflective" algorithm[21]. The algorithm requires a gradient vector and a Hessian matrix at each iteration evaluated at a specific design point[25]. The nature of the cost function $\bar{\tau}$ in the neighbourhood of a specific design point is approximately modelled using these gradient matrices. This approximate model is called a 'trust-region' . It reflects the behaviour of the actual function $\bar{\tau}$. The aim is then to minimise the cost function. Therefore a new design

point at which the "trust-region" reaches the minimum value is obtained. For instance, if $\bar{\tau}(\sigma_j) < \bar{\tau}(\sigma_i)$, then σ_j becomes the new point and the process continues. The functional tolerance value is calculated at each iteration and the process terminates when the tolerance value reaches a set minimum value.

Multi-objective Optimisation In this section, another GA based multi-objective optimizer is presented, called *gamultiobj*[25] . It performs a minimization of a vector of conflicting objectives subjected to constraints. Unlike a single-objective optimisation, in a multi-objective approach two conflicting objective functions, $\bar{\tau}_1$ and $\bar{\tau}_2$, are evaluated at the same time to find the set of optimal solutions. The multi-objective optimisation problem solved in this section is defined as

$$\begin{aligned} \min \quad & \bar{\tau}_{1,2}(\sigma), \\ & \sigma_l \leq \sigma \leq \sigma_u, \end{aligned} \tag{23}$$

where $\bar{\tau}_1$ is the average normal incidence reflection coefficient for a frequency range $[f_i, f_j]$ and $\bar{\tau}_2$ is the average normal incidence reflection coefficient for a frequency range $[f_k, f_l]$. Here, σ_l is the lower bound and σ_u is the upper bound of the optimisation problem as shown in **Figure 6**.

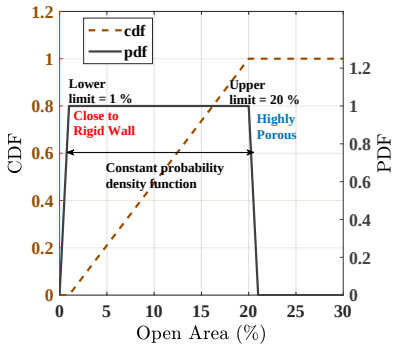

Figure 6. Probability and cumulative distribution of initial population (POA of the perforated layer).

Figure 7 presents a schematic of ideal multi-objective optimal solutions. The search for optimum solutions starts from an initial population of p individuals. All of the individuals of the initial population are evaluated. Each individual of a population is assigned a fitness or rank equal to its non-domination level and sorted on the basis of the non-domination level. The solutions/individuals which are not dominated by any other members of the set are called the non-dominated solutions. This set of non-dominated optimal solutions are called the Pareto optimum (dashed line in **Figure 7**) and it constitutes the basis in the multi-objective optimisation. Like a single-objective solver, a multi-objective algorithm creates a new set of populations from a subset of individuals with the best ranking of the current *population* through mutation and cross-over processes[25]. The children are ranked based on their objective function values and feasibility. Then, the current population and the children are combined into one matrix. Individuals of this matrix are sorted based on their rank and this procedure is iterated until the solver reaches one of the stopping conditions[20,22,25]. Due to the computational cost, a population of size 100 is evaluated for 3 generations. Earlier work has shown this number to be sufficient[21]. In this

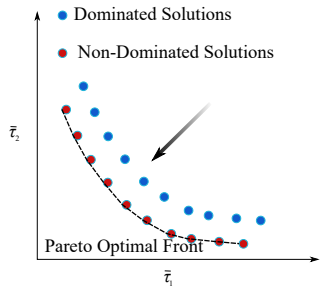

Figure 7. Probability and cumulative distribution of initial population (POA of the perforated layer).

procedure, the Pareto-optimal solutions are processed further to arrive at a single preferred solution based on the liner absorption requirements.

Novel Acoustic Liners

In this section, geometries are presented of three novel liner configurations designed for broadband attenuation: configuration 1 - partly perforated slanted septum; configuration 2 - slanted septum with two different percentage open areas; and configuration 3 - Multiple FOlded CAvity Liner (MultiFOCAL).

Configuration 1: Slanted Septum Core with Partial Perforation

An acoustic liner with a partly perforated slanted septum is shown to increase the acoustic propagation path length for low frequency sound waves. A schematic of the partly perforated slanted septum liner is shown in **Figure 8**. The baseline for this liner geometry is from a liner concept that was previously developed by Pongratz et al.[26] with an significant improvement of the broadband attenuation by applying a porous slanted septum suggested by Murray[27]. By using a partly perforated slanted septum, the effective cavity depth is increased. The POA of the face sheet and septum are optimized for maximum sound absorption for both the low and high frequency regime. The optimum effective POA of the face sheet and septum is observed to approach the required panel resistance and reactance for maximum normal incidence absorption at the targeted frequency regions (approaching R = 1, X = 0).

As shown in **Figure 8**, L_1 and L_2 denote the length of the resistive layer and interior hard-wall along the liner diagonal, respectively. The ratio L_1/L_2 is denoted by r and set to 0.5. The depth (H_c) of the liner is set to 60 mm. The width (w) of the liner is set to 29 mm. The hole diameter and sheet thickness are set to 0.8 mm and 1 mm, respectively.

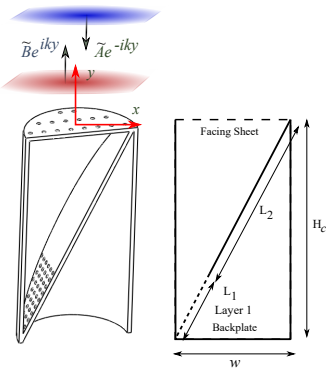

Figure 8. Geometry of optimised novel liner configuration 1. The length of the resistive layer L_1 = 22.2 mm and the interior hard-wall L_2 = 44.4 mm.

Once the novel design is set, the *gamultiobj* optimisation solver is used to investigate the acoustic performance of this novel liner with variations of the porosity of the face sheet (σ_{FS}) and diagonal septum (σ_1 – layer 1) through the optimisation procedure. In the first step, the total number of populations and generations are set to 100 and 2, respectively. With a large population size, the genetic algorithm searches the solution space thoroughly, thereby reducing the chance that the algorithm returns a local minimum that is not the global minimum. However, a large population size also causes the algorithm to run more slowly. Pure tone plane waves with a frequency in the range from 400 to 6000 Hz (in step of 100 Hz), and at a sound pressure level of 150 dB, are normally incident on the liner face sheet. The open area

of the liner face sheet and the diagonal septum are constrained within the range of 1 % (approaching hard-wall) to 20 % (highly-porous surface). In this optimisation, the hole diameter and the thickness of the face sheet and the diagonal layer are chosen to cover the range of interest applicable for aero-engine nacelle integration.

The objective functions for the low frequency regime($\bar{\tau}_1$) is

$$\bar{\tau}_1 = \frac{1}{(900-400)} \int_{400}^{900} |\tilde{\tau}\,(f)\,| df \tag{24}$$

and for the high frequency regime ($\bar{\tau}_2$),

$$\bar{\tau}_2 = \frac{1}{(4000-2000)} \int_{2000}^{4000} |\tilde{\tau}\,(f)\,| df \tag{25}$$

are calculated using the COMSOL FE model. The results obtained from the GA are superimposed on independently computed contours of the cost function in the σ_{fs}-σ_1 design space for validation.

Figure 9a shows the result of a multi-objective GA optimisation in the low frequency range for the partly perforated slanted septum liner. The contour plot indicates the evaluation of the objective function given by Equation 24, carried out independently in the (σ_{FS},σ_1) design space. The design variables corresponding to Pareto-optimum solutions are represented by the solid red dots. The objective functions $\bar{\tau}_1$ and $\bar{\tau}_2$ are evaluated 200 times in a *gamultiobj* solver in order to converge to the optimum Pareto front. The blue hollow circle indicates the optimum design value for maximum sound absorption in the low frequency regime. The optimum high frequency solution is also shown for comparison. It is clear that different designs are defined for the two frequency ranges.

In **Figure 9b**, results are presented of a multi-objective GA optimisation in the high frequency range for the partly perforated diagonal septum liner. The contour plot indicates the evaluation of the objective function $\bar{\tau}_2$ carried out independently in the (σ_{FS},σ_1) design space. The green hollow circle indicates the GA optimum design value for maximum sound absorption in the high frequency regime.

Configuration 2: Slanted Septum Core with Variable POA

As shown in **Figure 10**, configuration 2 is comprised of a slanted septum of total length $L_1 + L_2$, with different percentage of open areas in the two parts of the septum layer. The baseline for the geometry of the slanted septum core with different percentage open areas arises again from the liner concept previously patented by Murray[27]. The addition of perforations to the interior sound hard-wall part of the septum L_2 of configuration 1 provides an additional path for the incident sound. The introduction of an additional resistance and reactance are used to improve the sound absorption over a much broader frequency range compared to configuration 1. The length of the resistive layer 1 and 2 is equal to 22.2 mm and 44.4 mm respectively. The angle between the diagonal layer and the vertical wall are held constant and set to 25.8^o. The depth (H_c) and width of the liner, along with the hole diameters and sheet thickness, is kept the same as that of configuration 1.

The multi-objective optimisation procedure is applied to optimize the efffective POA of the face sheet and resistive layer 1 and 2 in order to maximise the sound absorption capability of this novel liner concept. The diameter of the perforations is fixed to 0.8 mm. Similarly, the thickness of the face sheet and the resistive diagonal is fixed to 1 mm.

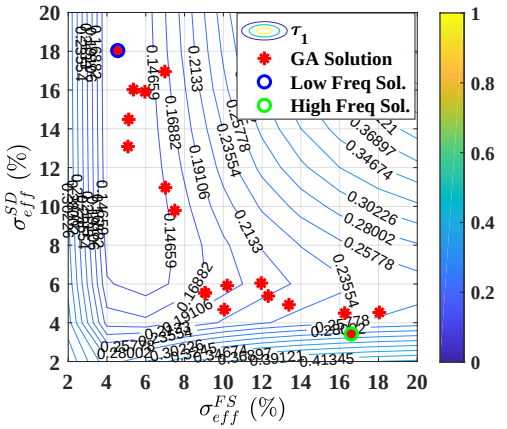

(a) Contour plot of the cost function $\bar{\tau}_1$ for low frequency (0.4 kHz - 0.9 kHz) optimum solution.

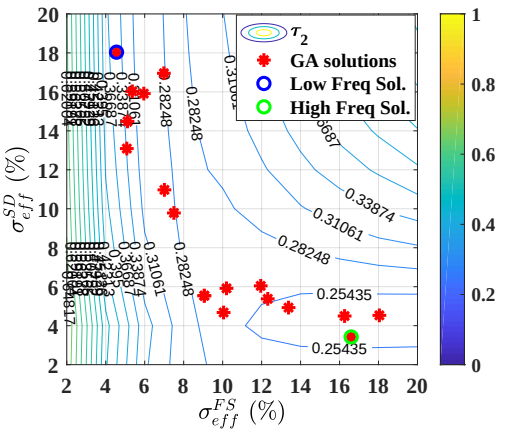

(b) Contour plot of the cost function $\bar{\tau}_2$ for high frequency 2 kHz - 4 kHz) optimum solution.

Figure 9. Results of *gamultiobj* optimisation of slanted septum core at 150 dB. Pareto-optimum design points (solid red circles), low frequency (hollow blue circle) and high frequency (hollow green circle) optimum design solution superimposed on pre-computed contours of the cost function in the (σ_{FS},σ_1) design space.

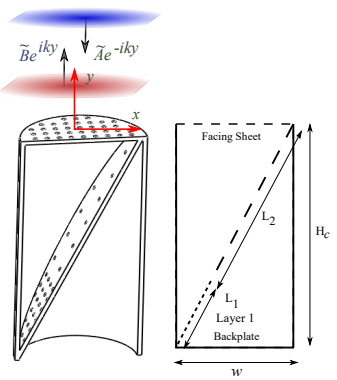

Figure 10. Geometry of slanted septum core with variable POA

In this case, the two objective functions to be minimized are

$$\bar{\tau}_1 = \frac{1}{(1000-400)} \int_{400}^{1000} |\tilde{\tau}(f)| \, \mathrm{d}f \,, \tag{26}$$

and

$$\bar{\tau}_2 = \frac{1}{(6000-2000)} \int_{2000}^{6000} |\tilde{\tau}(f)| \, \mathrm{d}f \,. \tag{27}$$

In **Figure 11**, the result of the GA multi-objective optimisation is presented. The objective functions,

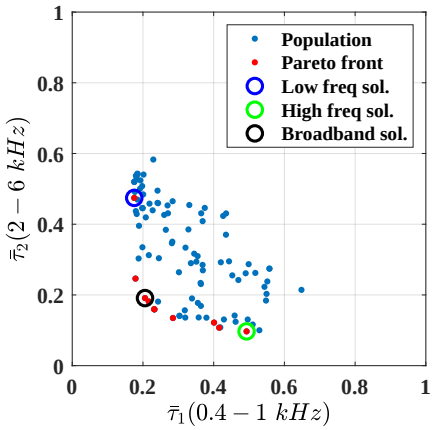

Figure 11. Results of *gamultiobj* optimisation of slanted septum core with variable POA at 150 dB. The objective values of Pareto-optimum design points (solid red circles), low frequency (0.4 kHz - 1 kHz) optimum solution represented by hollow blue circle, high frequency (2 kHz - 6 kHz) optimum solution represented by hollow green circle, and total population of 2^{nd} generation represented by solid light blue circles are superimposed.

as defined in Equation 26 and 27, are plotted against each other. A population size of 100 and 2 generations are used in this GA multi-objective optimisation. As mentioned earlier, three design variables are optimised. The Pareto front of these 3 variables and 2 cost functions optimisation problem have 10 design points (represented by red solid circles). The solid blue circles represent the cost function values of all the individuals in the second generation. The hollow blue circle represents the optimum design solution in the low frequency regime, 400–1000 Hz, providing maximum weighting to the objective function $\bar{\tau}_1$. The hollow green circle represents the optimum design solution in the high frequency regime, 2–6 kHz, providing maximum weighting to the objective function $\bar{\tau}_2$. The hollow black circle represents the broadband optimum solution, which is a trade-off between the low and high frequency solutions (minimum distance between tangent of Pareto front and the axis origin).

Configuration 3: Multiple FOlded CAvity Liner — MultiFOCAL concept

Figure 12 shows the geometry of a Multiple FOlded CAvity Liner, called the **MultiFOCAL** concept, based on the liner concept previously patented by Pool et al.[28] and Murray et al.[29]. The folded part of the segments are inclined at an angle of 58.8^o primarily to minimise complexity in the (planned) 3D printing. In addition to the folded segments, resistive septum layers are added inside the segments 1–5. The MultiFOCAL concept is expected to be better at all frequencies when compared to the previous liner configurations.

The width of each segment is 4.83 mm and assumed to be large enough to neglect the thermal and viscous losses. The centreline path length of segments 1–6 is gradually decreased from 79.8 mm to 14.7 mm. The individual values are listed in **Table 1**. The overall width (w) and depth (H_c) of the liner is 29 mm and 60 mm, respectively. The open area of the septa inside segments 2 to 5 is set initially to

20%, with very low non-linearity, and hence low acoustic resistance, at high SPL. Future iterations of this design will also include the septa open areas as optimisation design variables. The hole diameter (d_h) and sheet thickness (t_p) are set to 0.8 mm and 1 mm, respectively.

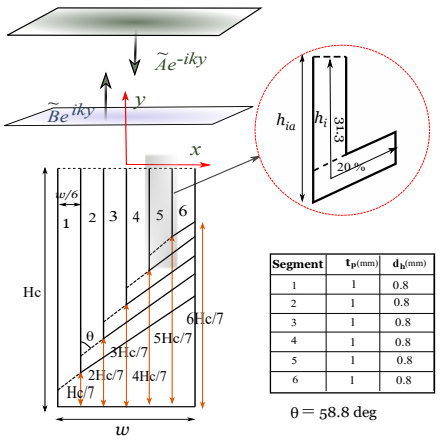

Segment	t_p(mm)	d_h(mm)
1	1	0.8
2	1	0.8
3	1	0.8
4	1	0.8
5	1	0.8
6	1	0.8

Figure 12. Geometry of MultiFOCAL concept.

Table 1. Depths of the segment of MultiFOCAL and the corresponding first quarter wave (QW) resonance frequencies.

Cavity	Centreline path length (h_i), mm	First QW Frequency, Hz
1	79.8	1065
2	75.3	1131
3	60.6	1405
4	45.9	1856
5	31.3	2721
6	14.7	5794

In this study, pure tone plane waves at a reduced sound pressure level 140 dB are normally incident on the MultiFOCAL surface in the frequency range from 0.4 to 6 kHz. The percentage open area of the face sheet of segments 1 to 6 and the septum of segment 1 are optimized using the single objective optimisation method. The main objective of the optimisation is to minimise the average coefficient of reflection ($\bar{\tau}$) for frequencies between 0.4 and 6 kHz. Therefore, the objective function to be minimized is

$$\bar{\tau} = \frac{1}{(6000 - 400)} \int_{400}^{6000} |\tilde{\tau}(f)| \, \mathrm{d}f \, . \tag{28}$$

The optimisation results are presented in **Figure 13**. A population size of 50 with 3 generations are selected for this study. **Figure 13a** indicates the evaluation points of the GA solver. The solid blue and

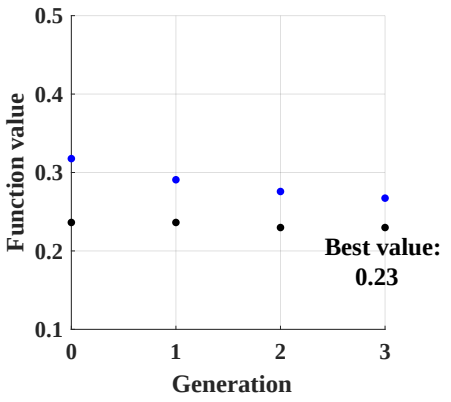

(a) Best (solid black circles) and average solution (solid blue circles) of each generation with a population size of 50.

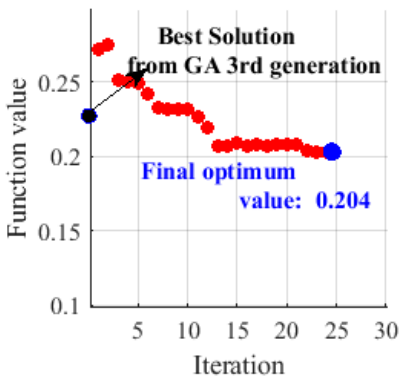

(b) Gradient-based local search of final optimum solution (solid blue circle) and the intermediate iterative solutions (solid red circles)

Figure 13. Results of hybrid optimisation of MultiFOCAL liner face sheet percentage open areas.

black circle indicates the average and the best value of the objective function, given by **Equation 28**, at each generation, respectively.

In **Figure 13b**, the pink solid circle indicates the value of the objective function at each iteration in the *fmincon* solver. The best solution in the 3^{rd} generation, represented by the black solid circle, is set as an initial value for the *fmincon* solver to perform an efficient local search. The blue solid circle indicates the final optimum value from the *fmincon* solver. In total, 200 evaluations are performed, in the GA optimiser, to reach the best solution and an additional 24 iterations, with 9 function evaluations for each iteration, are performed in *fmincon*[25] to converge to the final optimum value. The design variables (percentage open area) corresponding to the final optimum solution, represented by the blue solid circle in Figure 13b, are listed in **Table 2**.

Table 2. The percentage open area of the face sheet of segments 1–6 and the septum of segment 1 are optimized.

Segment	Optimum face sheet POA (σ_{fs}),%	Septum POA,%
1	15.3	3.6
2	15.7	20
3	9.9	20
4	16.2	20
5	18.4	20
6	18.1	-

Acoustic Properties of the Novel Liner Concepts

Slanted Septum Core: Optimum impedance and absorption coefficient

In **Figure 14a**, the predicted resistance, reactance, and absorption coefficient spectrum of the partly perforated diagonal septum liner are presented for the low frequency regime optimum solution (**Figure 9a**- blue circle). For $\sigma_{FS} = 4.5\,\%$ and $\sigma_1 = 18\,\%$, normal incidence absorption coefficient of at least 0.8 are observed in the frequency range of 400–1000 Hz. The first peak absorption for this liner configuration is located at ≈ 700 Hz, which falls within the targeted low-frequency range 400–900 Hz. The high POA of the septum ensures the liner behaves like a deep single layer folded cavity. The peak at 700 Hz corresponds to the quarter wavelength of the centreline of the folded path length (11.1 cm). This observation is reasonable as the highly porous septum is expected to enhance the absorption performance for the lowest frequencies by maximizing the acoustic path length for such low frequency waves to propagate. Also, good absorption of sound ($\alpha \geq 0.8$) is seen in another narrow bandwidth of frequencies in the range of 2000–2900 Hz. This is because the three-quarter wavelength of the longest centreline path length (11.1 cm) is at approximately 2300 Hz. At other frequencies between 900–2000 Hz and 3500–5000 Hz, the sound absorption is significantly less due to the presence of a strong anti-resonance inside the liner complex cavity at ≈ 1500 Hz, 3300 Hz and 4700 Hz. The first two frequencies correspond to effective single layer path lengths of approximately 11.1 cm and 5.2 cm, respectively, while the third represents the three-half wavelengths anti-resonance for the longest path length.

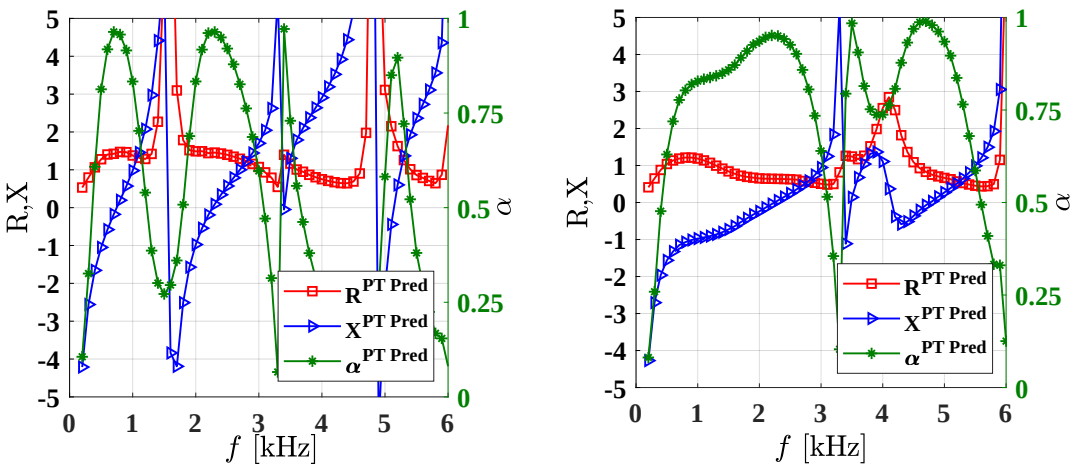

(a) Low frequency optimisation. σ_{fs} = 4.5 %, and σ_1 = 18 %

(b) High frequency optimisation. σ_{fs} = 16.6 %, and σ_1 = 3.4 %

Figure 14. Pure tone response of configuration 1 with optimized POA for low and high frequency sound absorption. Figure 14a and 14b — Resistance (red colour), Reactance (blue colour) and Absorption coefficient (green colour).

In **Figure 14b**, the predicted resistance, reactance, and absorption coefficient spectrum of the partly perforated diagonal septum liner are presented for the high frequency regime optimum solution

(**Figure 9b**-hollow green circle). For $\sigma_{FS} = 16.6\,\%$ and $\sigma_1 = 3.4\,\%$, a sound absorption coefficient of at least 0.8 is observed in the frequency range of 790 to 2800 Hz. The first peak of absorption for this high frequency optimum liner configuration is located at ≈ 2300 Hz corresponding to the three-quarter wavelength of the longest centreline path length (11.1 cm). Also, the low POA of the septum makes the cavity perform more like a double layer configuration. The absorption coefficient is good in another range of frequencies between 3400 and 5200 Hz. However, the anti-resonance corresponding to the initial 5.2 cm "cavity" remains, leading to a dip in the absorption spectra at 3300 Hz.

The sound absorption level spectra of the slanted septum layer liner for the low and high frequency optimum solutions calculated from Eqn. 20 are compared in **Figure 15**. It is shown that, generally, the higher the effective POA of the diagonal septum, the more the location of the first peak absorption is shifted towards lower frequencies. This is because the maximum available path length is used.

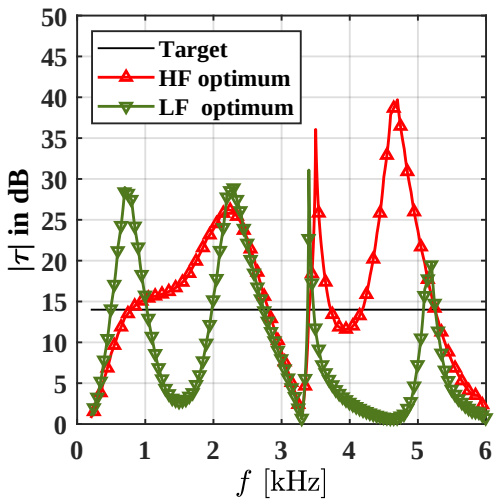

Figure 15. Sound absorption level comparison of the slanted septum core with optimum low and high frequency solutions. LF - optimum solution for low frequency regime (0.4–0.9 kHz), HF - optimum solution for high frequency regime (2–4 kHz)

Slanted Septum Core with Variable Open Area: Optimum impedance and absorption coefficient

In this section, the acoustic properties are presented of the slanted septum core with variable open area with effective percentage open areas optimized for low, high, and broadband frequency ranges. The optimum solutions at different frequency regimes are listed in Table 3.

For optimum low frequency absorption, the percentage open area of the face sheet and the resistive layers 1 and 2 are equal to $4.7\,\%$, $4.2\,\%$ and $14.6\,\%$, respectively. It has been shown previously that the non-linear resistance component at a given frequency is greatest for low open areas and high sound

Table 3. Optimum solutions from the Pareto front (Figure 11)

Frequency regime	σ_{fs},%	σ_1,%	σ_2,%	Cost Function, $\bar{\tau}_1$	Cost Function, $\bar{\tau}_2$
0.4–1 kHz	4.7	4.2	14.6	0.175	0.474
2–6 kHz	19.2	2.5	4.2	0.493	0.097
0.4–1 kHz and 2–6 kHz	10.3	8.6	1.6	0.206	0.191

pressure levels. With the optimum low frequency design solution, the desired resistance for the liner geometry is mainly generated by the face sheet and resistive layer 1, as opposed to resistive layer 2. It can be seen in **Figure 16a**, that the first peak in the absorption spectrum is at 920 Hz. This is because at 920 Hz the normalised reactance is 0 and the normalised resistance is ≈ 1.4, almost meeting the requirement for perfect absorption.

From the peak absorption frequency, the depth of an ideal quarter wave resonator (with $R = 1$ and $X = 0$) with a straight cavity (and zero face sheet inertance) can be directly estimated as

$$H_c = \frac{c_0}{4f} \tag{29}$$

where f is the first peak absorption frequency (taken from Figure 16a). Using $c_0 = 340.3m/s$ and $f = 920$ Hz yields a cavity depth of 92.4 mm, which is 54 % greater than the cavity depth (Hc). **Figure 16d** shows a comparison between the normal incidence sound absorption level for the slanted septum core with varying open areas optimised for low, high, and broadband frequency regimes. With the optimum low frequency liner, sound absorption of at least 14 dB is achieved in the frequency range of 570–1560 Hz, and the absorption decreases gradually due to the presence of an anti-resonance at 2500 Hz. By making layer 2 porous (upper diagonal), the strong anti-resonance observed in configuration 1 at 3300 Hz has been removed by the increased damping (compare with Figure 15).

The acoustic properties of the liner with a high frequency optimum design solution are presented in **Figure 16b**. For high frequency sound absorption, the optimum effective open areas obtained from the Pareto front of the GA multi-objective optimisation are $\sigma_{fs} = 19.2\,\%$, $\sigma_1 = 2.5\,\%$ and $\sigma_2 = 4.2\,\%$. The criterion used for this solution is to minimize the average coefficient of reflection ($\bar{\tau} < 0.2$) in the frequency range of 2–6 kHz. Unlike the low frequency design, the total resistance of this liner geometry is mainly generated by the (septum) resistive layers 1 and 2 rather than the face sheet. From **Figure 16b** and **Figure 16d**, it can be noticed that the first absorption peak is at 1.5 kHz, outside the targeted bandwidth. This complements the performance of the high frequency liner to ensure the normal incidence absorption level is above 15 dB over the frequency range of 1000–5500 Hz.

In terms of obtaining a trade-off between a low and high frequency solution, a broadband optimum design solution, $\sigma_{fs} = 10.3\,\%$, $\sigma_1 = 8.6\,\%$ and $\sigma_2 = 1.6\,\%$, has been sought based on the criterion of maximum allowable average coefficient of reflection $\bar{\tau}_{1,2} \leq 0.2$, in both of the frequency ranges (0.4–1 kHz and 2–6 kHz). **Figure 16c** shows the acoustic impedance and absorption spectra of configuration 2 with a broadband optimum solution. In **Figure 16d**, the normal incidence sound absorption level is shown for open areas optimised for broadband absorption. The resistive layer 2 is approaching a hard-wall condition. The first peak of absorption is at 920 Hz which is a characteristic feature of the optimum low frequency solution. Maximum sound absorption is at 920 Hz, 2500 Hz, 3500 Hz and 5200 Hz, where the normalised resistance and reactance values approach 1 and 0, respectively. The porous septum layer 2 helps to improve the overall panel absorption relative to that seen for configuration 1. It is noted,

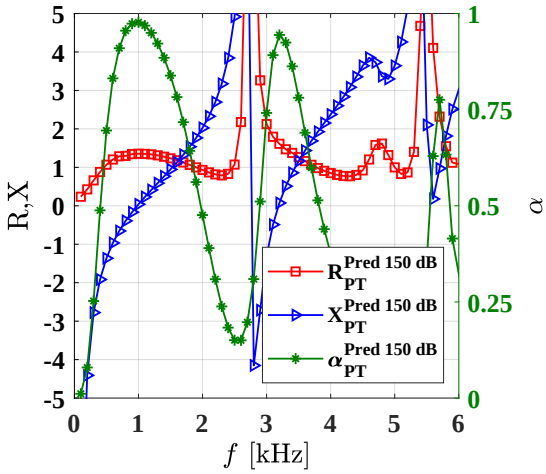

(a) Low frequency optimum solution. σ_{fs} = 4.7 %, σ_1 = 4.2 % and σ_2 = 14.6 %.

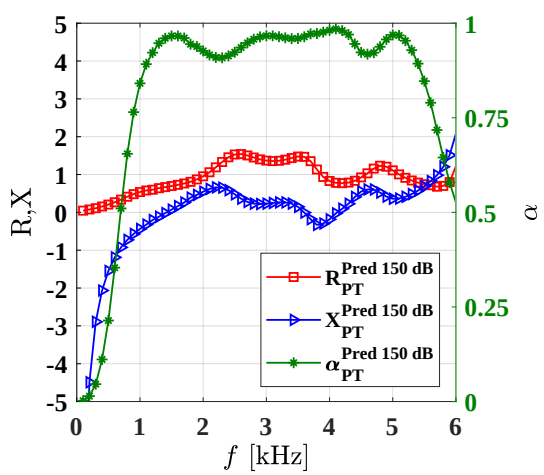

(b) High frequency optimum solution. σ_{fs} = 19.2 %, σ_1 = 2.5 % and σ_2 = 4.2 %.

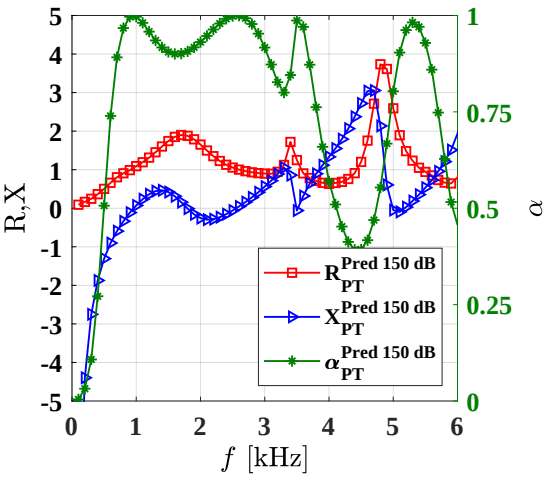

(c) Broadband optimum solution. σ_{fs} = 10.3 %, σ_1 = 8.6 % and σ_2 = 1.6 %.

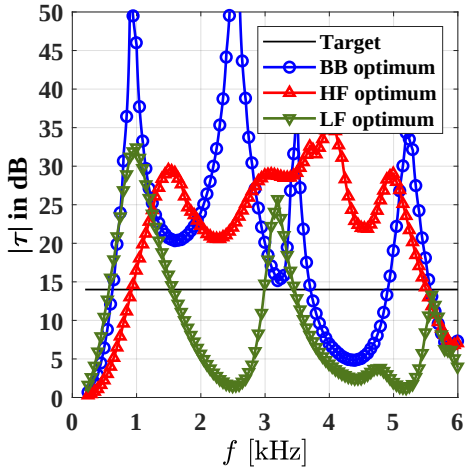

(d) Sound absorption level comparison of the slanted septum core with varying open areas.

Figure 16. Acoustic properties of novel liner configuration 2 optimized for low, high, and broadband frequency sound absorption with Pure Tone (PT) source. Figure 16a, Figure 16b, and Figure 16c - Resistance (red colour), Reactance (blue colour) and Absorption coefficient (green colour). Figure 16d LF — optimum solution for low frequency regime (0.4 – 1 kHz), HF — optimum solution for high frequency regime (2 – 6 kHz), and BB — optimum solution for broadband frequency regime (0.4 – 1 kHz and 2 – 6 kHz).

however, that the wide broadband requirement is difficult to achieve at all frequencies with this design, as evidenced by the dip in absorption at around 4300 Hz.

MultiFOCAL: Optimum impedance and absorption coefficient

Figure 17a shows the predicted acoustic properties of the optimum MultiFOCAL liner geometry for 140 dB pure tone excitation. The optimum percentage open area of the face sheet of segments 1–6 and the septum of segment 1, listed in Table 2, are used in the calculations. The first absorption peak is located at 0.6 kHz. However, the absorption coefficient at 0.6 kHz is relatively low and equals 0.6. Although the panel's normalised resistance is close to unity, the normalised reactance is ≈ -2. The other peaks in the absorption spectra are located at 1.2, 2, 3.5, 4.3 and 5 kHz where the coefficient of absorption are atleast equal to 0.90 or close to 1. Also, there are two small dips in the absorption spectra at 2.8 kHz and 4 kHz.

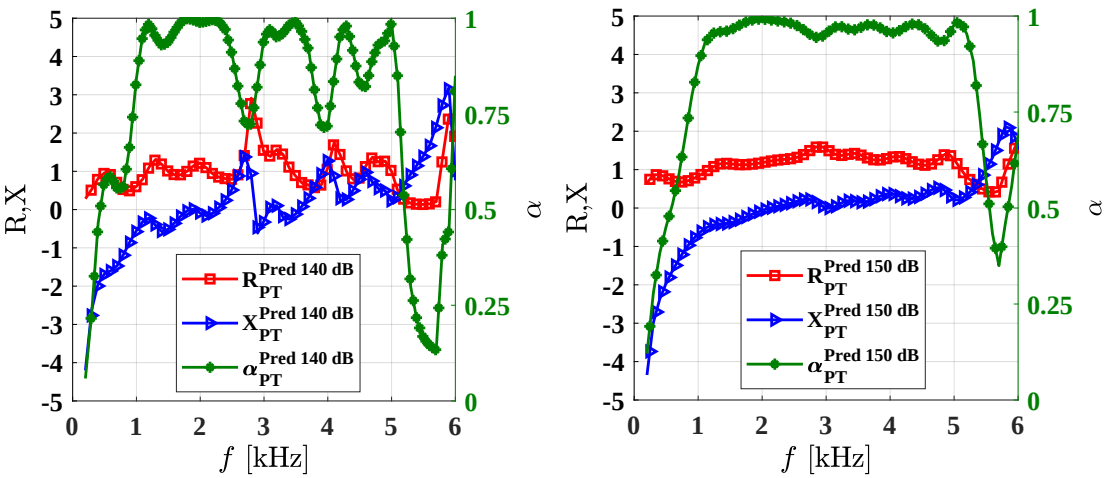

(a) Pure tone response at 140 dB. **(b)** Pure tone response at 150 dB.

Figure 17. Acoustic properties of the MultiFOCAL optimized for broadband sound absorption. Refer to Table 2 for design variables optimised at 140 dB. Resistance (red coloured squares), Reactance (blue coloured triangle) and Absorption coefficient (green coloured solid circle).

Figure 17b shows the acoustic properties predicted on the surface of the MultiFOCAL configuration when the liner is excited by pure tone plane waves at 150 dB. A higher level pure tone source is used to assess the robustness of the design. It can be seen that a high absorption coefficient (greater than 0.94) is maintained over a wide frequency band (0.9–5.3 kHz). The normalized resistance and reactance are close to 1 and 0, respectively, for most of the frequencies in the range of 0.9 to 5.3 kHz. The six closely packed peaks are broadened due to the general increase in the resistance, damping the anti-resonances, and flattening the normalised reactance curve towards 0. The resistance of the liner surface is mainly controlled by the septum (septum 1) of segment 1. This is because the optimum percentage open area of septum 1 is low compared to the face sheet of segments 1–6. Therefore, it has a significant non-linear impedance component at high sound pressure levels for such a low POA.

Figures 18 shows the normal incidence absorption level comparison of the MultiFOCAL design at 140 and 150 dB, for frequencies between 0.1 kHz and 6 kHz. As mentioned earlier, the narrow absorption peaks seen with 140 dB excitation broaden with 150 dB excitation. For frequencies between 1 kHz

and 5.1 kHz, the predicted MultiFOCAL absorption level is at least 14 dB, except for two small dips at 2.8 kHz and 4 kHz. For frequencies below 1 kHz, the acoustic performance of the MultiFOCAL configuration is relatively poor.

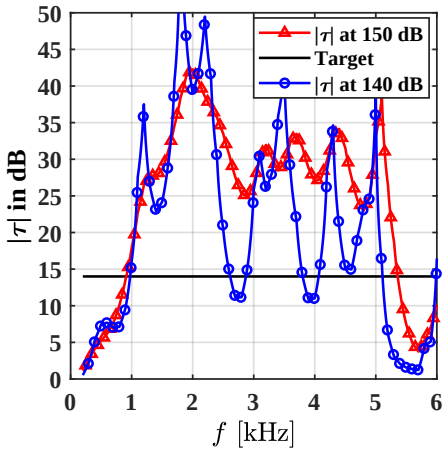

Figure 18. Comparison of modulus of reflection coefficient, in dB, of the MultiFOCAL concept for pure tone excitations at 140 dB and 150 dB. Attenuation spectra at 150 dB (green line), Attenuation spectra at 140 dB (red line), Target (black line).

Conclusion and Summary

This work presents a detailed numerical optimisation and investigation into the design of novel liner geometries for broadband sound absorption at normal incidence in the absence of grazing flow. A two-dimensional COMSOL FE model of a normal incidence impedance tube has been developed to predict the acoustic properties of the liners. In the FE model, semi-empirical equations are applied as interior boundary conditions to translate physical parameters of the face sheet and septum into normalised resistance and reactance. The semi-empirical equations include only the effects of liner face sheet geometry and the incident sound pressure level of pure tones. It does not include the effects of grazing flow, as the initial aim of this research is to investigate the design of novel acoustic liners with maximised sound absorption at high SPL with normally incident, pure tone, acoustic plane waves. The design challenge is focussed on the cavity geometry needed to realise optimum reactance characteristics. Once the reactance spectrum is optimised, it is then a relatively straightforward task to adjust the face sheet geometry in order to realise the desired liner impedance under grazing flow.

A hybrid optimisation procedure has been presented where the objective functions evaluated by the COMSOL FE model are defined within a MATLAB optimisation solver. The optimisation technique involves a combination of a global GA search and a local gradient-based search algorithm. The percentage open areas of various resistive layers were optimised to minimize the normal incidence complex reflection coefficient at high SPLs for pure tone acoustic plane waves. The numerical results show the predicted benefit of using complex cavities with resistive septum layers for maximisation of sound absorption. It

is also shown that the sound absorption capability of the optimised novel liners is predicted to be more broadband when the incident sound pressure level is increased, due to an increase in resistance and a reduction in reactance over a wide range of frequencies. This is due to the non-linear behaviour of the perforates attributed to the vortex shedding at the entrance and exit of the orifices, which were considered in this numerical modelling. This confirms that such effects cannot be neglected while designing liners for high SPLs.

Summary of liner modelling in COMSOL

The following points provide a summary of the two-dimensional normal incidence impedance tube model used to predict the resistance and reactance of acoustic liners in a quiescent medium:

1. The acoustic energy dissipation mechanism is primarily comprised of two components: (1) the direct viscous dissipation in the openings of the face sheet at low SPL, and (2) the dominant shedding of vortices from the edges of the openings at medium and high SPL.
2. The normalised resistances and reactances are computed by solving the Helmholtz equation for a given liner geometry and frequency. The perforated resistive layers are modelled as an impedance boundary condition. The model accurately predicts the acoustic properties when compared with experimental data.
3. The detailed numerical study outlined in this article has provided guidance on the optimisation of design parameters of liners and their influence on liner resistance and reactance.

Summary of novel liner design

Three novel liner geometries were designed and evaluated in order to maximise broadband sound absorption, namely a partly perforated slanted septum, a slanted septum with two different percentage open areas, and a Multiple FOlded CAvity Liner (MultiFOCAL). The following points provide a summary of the optimised novel liner acoustic performance in a quiescent medium:

1. The normal incidence sound absorption of the slanted septum core with partial perforation, over a relatively narrow low-frequency bandwidth, 400–1000 Hz, is predicted to be at least 0.8 when the percentage open area of the septum is sufficiently large compared to that of the face sheet, σ_{FS} = 4.5% and σ_1 = 18%. Such a high POA of the septum ensures the liner behaves like a deep single layer folded cavity at low frequencies. The presence of strong anti-resonances was also observed in this liner concept, at $\approx$ 1500 Hz, 3300 Hz and 4700 Hz, where the sound absorption deteriorated. These may only be removed by increased damping.
2. The slanted septum core with varying POA, with a broadband optimum solution: σ_{FS} = 10.3%, σ_1 = 8.6%, and σ_2 = 1.6%, improved the sound absorption when compared to the slanted septum core with partial perforation. The absorption maxima are located at frequencies 920 Hz, 2500 Hz, 3500 Hz and 5200 Hz, where the normalised resistance and reactance values approach 1 and 0, respectively. Also, the attenuation drops in between the peaks at 3500 Hz and 5200 Hz due to the presence of an anti-resonance at 4400 Hz. However, the same liner layout designed for a high frequency optimum solution: σ_{FS} = 19.2%, σ_1 = 2.5%, and σ_2 = 4.2%, provided an absorption coefficient of above 0.8 in the frequency range from 1000 to 5500 Hz.

3. Finally, the Multiple FOlded CAvity Liner (MultiFOCAL) concept is predicted to give the best broadband sound absorption for normally incident pure tone excitation. It is shown that the depth of each segment controls the sound absorption at selected frequencies corresponding to their quarter-wave resonance conditions. Also, it has been shown that the method of distributing the impedance over the surface of the liner panel improves sound absorption over a broad range of frequencies. With the MultiFOCAL concept, significant amount of normal incidence absorption are predicted at high SPL excitation in the frequency range from 900 to 5300 Hz.

It is noted that these liners are designed for normal incidence without grazing flow. The face sheet properties may subsequently be altered in order to maximise engine nacelle duct attenuation.

Acknowledgments

The work in this article is part of the ARTEM project. This project has received funding from the European Union's Horizon 2020 research and innovation programme under grant No 769 350. The authors wish to acknowledge the technical input to this work from Kylie Knepper (NLR). Also, the authors wish to acknowledge the continuing support provided by Rolls–Royce plc through the University Technology Centre in Propulsion Systems Noise at the Institute of Sound and Vibration Research.

References

1. Ingard U. On the theory and design of acoustic resonators. *The Journal of the Acoustical Society of America* 1953; 25(6): 1037–1061.
2. Melling T. The acoustic impendance of perforates at medium and high sound pressure levels. *Journal of Sound and Vibration* 1973; 29(1): 1 – 65.
3. Motsinger R and Kraft R. Design and performance of duct acoustic treatment. *Aeroacoustics of Flight Vehicles: Theory and Practice* 1991; 2(14): 165–206.
4. Hersh A, Walker B and Celano J. Effect of grazing flow and spl on impedance of 2-dof resonators. *8th AIAA/CEAS Aeroacoustics Conference* 2002; DOI:10.2514/6.2002-2443.
5. Tam CK, Ju H, Jones M et al. A computational and experimental study of resonators in three dimensions. *Journal of Sound and Vibration* 2010; 329(24): 5164 – 5193.
6. Murray P and Astley RJ. Development of a single degree of freedom perforate impedance model under grazing flow and high spl. *18th AIAA/CEAS Aeroacoustics Conference* 2012; DOI:10.2514/6.2012-2294.
7. Serrano PG, Gabard G, Murray PB et al. Non-linear interaction of multiple tones on perforated liners. *22nd AIAA/CEAS Aeroacoustics Conference* 2016; DOI:10.2514/6.2016-2790.
8. Serrano PG. *Measurement and prediction of nonlinear acoustic liners in the presence of high level multiple tones*. PhD Thesis, University of Southampton, 2018.
9. Jones MG and Parrott T. Parallel-element liner impedances for improved absorption of broadband sound in ducts. *Noise Control Engineering Journal* 1995; 43.
10. Howerton B and Parrott T. Validation of an acoustic impedance prediction model for skewed resonators ; DOI: 10.2514/6.2009-3143.
11. Schiller NH and Jones MG. Smeared impedance model for variable depth liners. *24th AIAA/CEAS Aeroacoustics Conference* 2018; DOI:10.2514/6.2018-3774.
12. Sugimoto R, Murray P and Astley R. Folded cavity liners for turbofan engine intakes. *18th AIAA/CEAS Aeroacoustics Conference* 2012; DOI:10.2514/6.2012-2291.
13. Nark DM and Jones MG. Design of an advanced inlet liner for the quiet technology demonstrator 3 ; DOI: 10.2514/6.2019-2764.
14. Jones M, Watson W, Nark D et al. A review of acoustic liner experimental characterization at nasa langley 2020; : 1–58.
15. Jones MG, Nark DM, Howerton BM et al. Uniform and multizone liner results for the international forum for aviation research. *AIAA AVIATION 2020 FORUM* 2020; DOI:10.2514/6.2020-2533.
16. COMSOL. Acoustics module user's guide. *Version 53a* 2017; .
17. Ingard U. Influence of fluid motion past a plane boundary on sound reflection, absorption, and transmission. *The Journal of the Acoustical Society of America* 1959; 31(7): 1035–1036.
18. Lafronza L, McAlpine A, Keane A et al. Response surface method optimization of uniform and axially segmented duct acoustics liners. *Journal of Aircraft* 2006; 43(4): 1089–1102.
19. Copiello D and Ferrante P. Multi-objective optimization of "true" zero-splice liners for aero-engine intakes. *15th AIAA/CEAS Aeroacoustics Conference* 2009; DOI:10.2514/6.2009-3107.
20. Deb K, Agrawal S, Pratap A et al. A fast elitist non-dominated sorting genetic algorithm for multi-objective optimization: Nsga-ii. *Parallel Problem Solving from Nature PPSN VI* 2000; : 849–858.
21. Astley R, Sugimoto R and Mustafi P. Computational aero-acoustics for fan duct propagation and radiation. current status and application to turbofan liner optimisation. *Journal of Sound and Vibration* 2011; 330(16): 3832–3845.

22. Sasaki D and Obayashi S. Efficient search for trade-offs by adaptive range multi-objective genetic algorithms. *Journal of Aerospace Computing Information and Communication* 2005; 2: 44–64. DOI:10.2514/1.12909.
23. Chambers AT, Manimala JM and Jones MG. Design and optimization of 3d folded-core acoustic liners for enhanced low-frequency performance. *AIAA Journal* 2020; 58(1): 206–218. DOI:10.2514/1.J058017.
24. Tissot G, Billard R and Gabard G. Optimal cavity shape design for acoustic liners using helmholtz equation with visco-thermal losses. *Journal of Computational Physics* 2020; 402: 109048.
25. MATLAB. Optimization toolbox. *The MathWorks, Natick, MA, USA* R2018a; .
26. Pongratz R, Richter C, Kern M et al. Sound absorber assembly. *Patent* 2016; (US9303588B2): 1 – 8.
27. Murray P. Sound absorber. *Patent-US2020/0141357* 2020; : 1–16.
28. Pool CL, Udall KF, Stretton RG et al. Duct wall for a fan of a gas turbine engine. *Patent- US 2010/0284790 A1* 2010; : 1–9.
29. Murray P, Astley R, Sugimoto R et al. An acoustic liner. *Patent- EP 2 466 095 A2* 2012; : 1–6.